

A diffusion-map-based algorithm for gradient computation on manifolds and applications

Alvaro Almeida Gomez^a, Antônio J. Silva Neto^b, Jorge P. Zubelli^{a,c,*}

^aIMPA, Est. D. Castorina, 110, Jardim Botânico, Rio de Janeiro, 22460-320, Brazil

^bIPRJ-UERJ, R. Bonfim 25, Nova Friburgo 28625-570, Brazil

^cKhalifa University, P.O. Box 127788, Abu Dhabi, UAE

Abstract

We recover the gradient of a given function defined on interior points of a submanifold with boundary of the Euclidean space based on a (normally distributed) random sample of function evaluations at points in the manifold. This approach is based on the estimates of the Laplace-Beltrami operator proposed in the theory of Diffusion-Maps. Analytical convergence results of the resulting expansion are proved, and an efficient algorithm is proposed to deal with non-convex optimization problems defined on Euclidean submanifolds. We test and validate our methodology as a post-processing tool in Cryogenic electron microscopy (Cryo-EM). We also apply the method to the classical sphere packing problem.

Keywords: Diffusion-Maps; Gradient operator; Gradient descent; Gradient flow; Machine learning; Non-convex optimization; Sphere packing; Cryogenic electron microscopy.

1. Introduction

Several iterative minimization algorithms in Euclidean spaces rely on the fact that the negative gradient determines the steepest descent direction. The applications in inverse problems and imaging abound [1]. Some examples of these algorithms are the Gradient Descent and Newton's method [2]. These methods can be generalized to Riemannian submanifolds of \mathbb{R}^n using a retraction function, as proposed in Refs. [3, 4]. An important task in these methods is to compute the gradient which is typically done in local coordinate charts. Often it is not easy to access the function's local behavior due to its complexity, as well as noisy measurements. Furthermore, factors such as noise can seriously modify

*Corresponding author

Email addresses: alvaro.gomez@ku.ac.ae (A. A. Gomez), ajsneto@iprj.uerj.br (A. J. Silva Neto), zubelli@gmail.com (J. P. Zubelli)

the estimates of the gradient. In Ref. [5], an estimate to compute the gradient is given. However, these estimates are based on solving an optimization problem, and also depend on the dimension of the submanifold.

The purpose of this article is to compute approximations of the gradient of a function on random sample of points without *a priori* knowledge of the submanifold's dimension. An important feature of our approximations is that they do not depend on convexity conditions of the function. This leads to a promising methodology to treat minimization problems involving Lipschitz functions defined in Euclidean submanifolds.

The main tool to compute these estimates is the Diffusion-Map theory. The latter is a dimensional reduction methodology which is based on the diffusion process in a manifold. See Refs. [6, 7, 8] for more details. An important feature of this theory is that it recovers the Laplace-Beltrami operator when the data set approximates a Riemannian submanifold of \mathbb{R}^n . The Diffusion-Map theory is based on a symmetric kernel defined on the data set. This symmetric kernel measures the probability that two points are locally connected. Our approach is based on implementing this theory in the recently developed case of asymmetric kernels [9]. Compared to symmetric kernels, asymmetric ones provide more details how the information is distributed along each direction. This characteristic allows to know which direction has the greatest variations.

We use these approximations as principal directions in a step size method. The main advantage of using these estimates is that it does not depend on a prior knowledge of the gradient of the function. Furthermore, these estimates are robust to noisy data. We apply our theory developed as a post-processing method in the cryogenic electron microscopy (Cryo-EM) reconstruction problem. This post-processing algorithm could be parallelizable and run in several computers or CPU's simultaneously. It also has a similar flavor of the algorithm developed in [10, 11] inasmuch as we are trying to solve a high dimensional optimization problem with a swarm of computed auxiliary data. In the latter case, this is done with the approximation to the roots of a high degree polynomial.

This paper is organized as follows, in Section 2, we state our main result and we give a brief exposition of the classical representation theory for diffusion distances proposed in Refs. [6, 7, 8]. In Section 3, we review facts about flows defined over manifolds, and we show how to use the flow generated by the approximations to find minimizers. In Section 4, we show some experiments on the sphere, and we also show the effectiveness of our reconstruction method in the Cryo-EM problem. Finally, in Appendices A and B we cover the technical details of proof of the main result.

2. Diffusion-Maps

In this section, we review some facts on diffusion map theory. We refer the reader to Refs. [6, 7, 8] for more details. Diffusion maps is a dimensionality reduction method that is based on the diffusion process over data sets. The diffusion process is described using a positive real symmetric kernel which measures the local connectivity of the data points. In our approach we generalize this methodology to asymmetric vector value kernels. The main advantage of using these kernels is that we have a more specific description of the distribution of data set in certain directions. Based on the expansion for the Laplace-Beltrami operator proposed in Ref. [6] we recover the gradient operator. First, we consider the vector-value kernel

$$\overline{K}_t : \mathcal{M} \times \mathcal{M} \rightarrow \mathbb{R}^n,$$

defined as

$$\overline{K}_t(x, y) = (y - x)e^{\frac{-\|y-x\|^2}{2t^2}}.$$

Assume that $\frac{1}{2} < \delta < 1$, and let $d_t(x)$ be defined by

$$d_t(x) = \int_{U(x, t^\delta)} e^{\frac{-\|y-x\|^2}{2t^2}} dy,$$

where

$$U(x, t) = \{y \in \mathcal{M} \mid \|y - x\| \leq t\}. \quad (2.1)$$

We consider the Markov normalized kernel given by

$$\rho_t(x, y) = \frac{\overline{K}_t(x, y)}{d_t(x)}.$$

For a function f , we define the operator

$$\overline{P}_t f(x) = \int_{U(x, t^\delta)} \rho_t(x, y) (f(y) - f(x)) dy. \quad (2.2)$$

This operator approximates the gradient of a function without explicitly referring to the dimension of the manifold. This fact is established in the following result. The technical details of the proof of this result are shown in Appendices A and B.

Theorem 2.1. *Let \mathcal{M} be a Riemannian submanifold of \mathbb{R}^n and assume that the function*

f is smooth at the interior point x . Then, we have that

$$\lim_{t \rightarrow 0} \frac{\overline{P}_t f(x)}{t^2} = \nabla f(x). \quad (2.3)$$

Note that the operator does not depend on some differentiability condition. Furthermore, since the operator is defined as an integral, then it is robust to noisy measurements. Considering these characteristics, we use the operator $\overline{P}_t f(x)$ instead of the gradient in the step size method.

3. Flows and optimization methods on submanifolds

3.1. Flows on manifolds

In this section, we review some facts of flows defined on submanifolds, and we show how these flows can be used in optimization methods. Assume that $h : \mathcal{M} \rightarrow \mathbb{R}^n$ is a continuous function defined on the submanifold $\mathcal{M} \subset \mathbb{R}^n$. We say that a curve b starts at x_0 , if $b(0) = x_0$. The Peano existence theorem guarantees that for all $x_0 \in \mathcal{M}$, there exists a smooth curve $c_{h,x_0} : (-\varepsilon, \varepsilon) \rightarrow \mathcal{M}$ starting at x_0 , which is solution of

$$c'_{h,x_0}(s) = -h(c_{f,x_0}(s)). \quad (3.1)$$

We refer the reader to Ref. [12] for a complete background about ordinary differential equations. We observe that assuming only the continuity condition, the uniqueness of the curve is not guaranteed. Since the solution of Eq. (3.1) is not unique, we can concatenate solutions as follows. Let c_{h,x_0} be a solution of Eq. (3.1) starting at the point x_0 . For a fix s_1 in the domain of c_{h,x_0} , we define $x_1 = c_{h,x_0}(s_1)$. If c_{h,x_1} is a solution of Eq. (3.1) starting in x_1 , we define a new curve c_{h,x_0,x_1} as

$$c_{h,x_0,x_1}(s) = \begin{cases} c_{h,x_0}(s), & \text{for } s \leq s_1 \\ c_{h,x_1}(s - s_1), & \text{for } s_1 < s \end{cases}.$$

Proceeding recursively, we obtain a piecewise differentiable curve $c_{h,x_0,x_1,x_2,\dots}(s)$ starting at x_0 , and satisfying Eq. (3.1) (except in a discrete set). See Figure 3.1 for a graphic description. In this case, we say that the curve $c_{h,x_0,x_1,x_2,\dots}(s)$ is a piecewise solution of Eq. (3.1). We focus on curves which are solutions (except in a discrete set) of Eq. (3.1), because these curves allow updating the direction in which we look for stationary points.

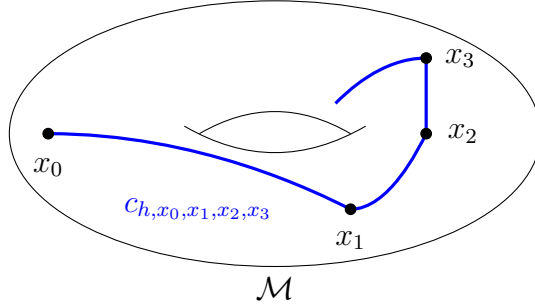


Figure 3.1: Piecewise curve obtained by concatenating three curves.

3.2. Gradient Flow

Suppose that $f : \mathcal{M} \rightarrow \mathbb{R}^n$ defines a smooth function. In this case we consider the vector field $h = \nabla f$. If $c_{h,x_0,x_1,x_2,\dots}$ is a piecewise solution of Eq. (3.1) starting at x_0 . Then, for all t (except in a discrete set), we have that

$$(c'_{h,x_0}(s))^2 = -\frac{d}{ds}f(c_{f,x_0}(s)). \quad (3.2)$$

Therefore, the function $f(c_{f,x_0}(\cdot))$ is decreasing. Thus, if we move through time, we can find a better approximation for the minimizer.

3.3. Lipschitz functions

We say that f is locally Lipschitz function if for all $x \in \mathcal{M}$ there exists a neighbourhood $x \in U \subset \mathcal{M}$ and a positive constant C , such that for all $y \in U$ satisfies

$$\|f(x) - f(y)\| \leq C\|x - y\|.$$

We also recall that the Sobolev space $H^1(0, T, \mathcal{M})$ is defined as the set of all integrable functions from $[0, T]$ to \mathcal{M} whose weak derivative is also integrable in the L^2 norm.

Our goal is to use the previous approach to find minimal points of locally Lipschitz functions. Rademacher's theorem states that the gradient operator ∇f exists almost everywhere. See Ref. [13] for more details. However, for a locally Lipschitz function f the gradient ∇f may not exist for all points. In this case, it is not possible to define the gradient flow.

To deal with this problem, we propose to use the flow generated by approximation $\frac{\bar{P}_t f(x)}{t^2}$ defined in Eq. (2.2) instead of the gradient flow. The operator $\bar{P}_t f$ is defined as an integral, then it is continuous. This fact guarantees the existence of a flow associated with $\frac{\bar{P}_t f(x)}{t^2}$, for arbitrarily small positive t .

Now we show that at the points where the function is smooth, this flow approximates a curve in which the function decreases with time. To do that, we first test a technical result.

Proposition 3.1. *Suppose that f is continuously differentiable in an open neighbourhood of x_0 . We define the function $J : [0, T] \times \overline{B(x_0, R)} \cap \mathcal{M} \rightarrow \mathbb{R}^n$ as*

$$J(t, x) = \begin{cases} \frac{P_t f(x)}{t^2}, & \text{for } 0 < t \\ \nabla f(x), & \text{for } t = 0 \end{cases}.$$

Then, for small enough numbers T, R , the function J is uniformly continuous. In particular, there exists a positive constant M such that for all $(t, x) \in (0, T] \times \overline{B(x_0, R)} \cap \mathcal{M}$ the following estimate holds.

$$\frac{P_t f(x)}{t^2} \leq M.$$

Proof. Since the set $[0, T] \times \overline{B(x_0, R)} \cap \mathcal{M}$ is compact, it is enough to show that J is continuous. Observe that for $0 < t$ the following estimate holds

$$\|\rho_t(x, y)(f(y) - f(x))\| 1_{U(x, t^\delta)}(y) \leq C t^{2\delta} e^{\frac{-\|y-x\|^2}{2t^2}} \frac{1}{d_t(x)}.$$

Since the function $e^{\frac{-\|y-x\|^2}{2t^2}} \frac{1}{d_t(x)}$ is integrable on the variable y , and since the function

$$(t, x) \rightarrow \frac{\rho_t(x, y)(f(y) - f(x))}{t^2} 1_{U(x, t^\delta)},$$

is continuous, then, by the dominated convergence theorem we conclude that the operator $J(t, x)$ is continuous on $(0, T] \times \overline{B(x_0, R)} \cap \mathcal{M}$.

On the other hand, using Estimate (B.1) of the proof of Theorem 2.3 and Lemma B.2, we conclude that the function J is continuous for all points of the form $(0, x)$. This proves our result. \square

The estimate of Proposition 3.1 states that for a fixed x_0 , and small T , the family of curves $\{c_{h(t_n), x_0}\}_{t_n}$ is uniformly bounded on the Sobolev space $H^1(0, T, \mathcal{M})$. Therefore, for any sequence $t_n \rightarrow 0$, there exists a subsequence $t_{n_k} \rightarrow 0$ such that $c_{h(t_{n_k}), x_0}$ converges weakly to some $c \in H^1(0, T, \mathcal{M})$. Observe that by Arzela Ascoli theorem, we can also

suppose that the sequence $c_{h(t_n),x_0}$ converges uniformly to c . Finally we prove the following result.

Proposition 3.2. *Assume the same assumptions, and notation of Proposition 3.1. Then, for $t_1 < t_2$ we have that*

$$f(c(t_1)) \geq f(c(t_2)).$$

Proof. Proposition 3.1 states that for all t_{n_k} the image $c_{h(t_{n_k}),x_0}(I)$ lies in the ball $B = B(x_0, CT)$. We claim that $\frac{\overline{P}_t f(c_{h(t_n),x_0}(\cdot))}{t^2}$ converges pointwise to $\nabla f(c(\cdot))$. In fact, for $s \in I$, we have by Proposition 3.1 that

$$\lim_{n \rightarrow \infty} \frac{\overline{P}_t f(c_{h(t_n),x_0}(s))}{t^2} - \nabla f(c_{h(t_n),x_0}(s)) = 0.$$

The continuity of the gradient guarantees that

$$\lim_{n \rightarrow \infty} \nabla f(c_{h(t_n),x_0}(s)) - \nabla f(c(s)) = 0.$$

The above estimates prove our claim. Therefore, by the dominated convergence theorem we obtain that

$$\lim_{n \rightarrow \infty} \int_0^T \left\| \frac{\overline{P}_t f(c_{h(t_n),x_0}(s))}{t^2} - \nabla f(c(s)) \right\|^2 ds = 0. \quad (3.3)$$

On the other hand, since $c_{h(t_n),x_0}(I)$ is solution of Eq. (3.1), we have that

$$\begin{aligned} 0 &\geq \left\langle \frac{\overline{P}_t f(c_{h(t_n),x_0}(s))}{t^2}, c'_{h(t_n),x_0}(s) \right\rangle \\ &\geq \left\langle \frac{\overline{P}_t f(c_{h(t_n),x_0}(s))}{t^2} - \nabla f(c(s)), c'_{h(t_n),x_0}(s) \right\rangle + \left\langle \nabla f(c(s)), c'_{h(t_n),x_0}(s) - c'(s) \right\rangle \\ &+ \left\langle \nabla f(c(s)), c'(s) \right\rangle. \end{aligned}$$

Using the weak convergence assumption, together with Eq. (3.3), we conclude that for all points $t_1 < t_2$, the following inequality holds

$$0 \geq \int_{t_1}^{t_2} \left\langle \nabla f(c(s)), c'(s) \right\rangle ds = f(c(t_2)) - f(c(t_1)).$$

□

4. Algorithm Development

In this section we propose a computational algorithm that optimizes Lipschitz functions on Euclidean submanifolds. We assume that the function is smooth except in a discrete set. We say that a point is a singularity if it is in the latter set.

Proposition 3.2 says that the energy of the gradient decreases along the curve c . Therefore, we can use this curve to find a better approximation for the minimizer ultimately leading to a computational algorithm. In fact, in practical situations, it might not straightforward to compute the gradient of a function. This is due to factors such as complexity and noise. Thus, we propose an alternative step size method based on Proposition 3.2. It states that the flow generated by

$$Dir = \frac{\overline{P}_t f(x)}{t^2}, \quad (4.1)$$

approximates a curve along which the function f decreases. Thus suggesting that if we use the direction Dir defined in Eq. (4.1) in an adaptive step size, then in a certain way we are approximating the descending gradient method. The parameter t will control how much we will approximate the true gradient. Needless to say, a choice of extremely small t would lead to numerical instabilities, and thus t in a certain sense would work as a regularization parameter. We shall call t the *gradient approximation parameter* and it will be provided as a input to the algorithm.

We recall that a local retraction β consists of a locally defined continuous map from the ambient space onto the manifold \mathcal{M} such that it coincides with the identity when restricted to \mathcal{M} . In other words, $\beta \circ \iota = I_A$, where A is a open set in \mathcal{M} , and ι is the inclusion map from \mathcal{M} into the ambient space. The flow generated by direction Dir can be described using Euler's method

$$x_{k+1} = \beta_{x_k}(x_k - \lambda \frac{\overline{P}_t f(x_k)}{t^2}),$$

where λ is the relaxation parameter which defines the step size, and β_x a local retraction of \mathcal{M} around the point x . The parameter λ must be regularly reduced to avoid instabilities in our iteration. We propose to reduce the *relaxation parameter* λ by a step-scale factor s_f after l consecutive numerical iterations. We shall call l the *sub-iteration control number*.

An important task is to compute the integrals involving the operator \overline{P}_t . In practical applications, we only have access to measurements on a finite sample of data points which approximate the manifold \mathcal{M} . We use Monte Carlo approach to estimate the inte-

grals using sample points. We endow the manifold \mathcal{M} with the density function $q(y) = 1_{U(x,t)}(y)e^{\frac{-\|y-x\|^2}{2t^2}}/d_t(x)$, And we approximate the integrals as follows. If $x_1, x_2, x_3 \cdots x_m$ are i.i.d realizations with density q , then the law of large numbers states that for m large

$$\overline{P}_t f(x) \approx \frac{1}{m} \sum_{i=1}^m (x_i - x)(f(x_i) - f(x)).$$

In the following experiments, we use the above expression to compute \overline{P}_t . For practical purposes we generate random points on \mathcal{M} as follows. First, we generate normal random points $s_1, s_2, s_3 \cdots s_m$ in \mathbb{R}^n with mean x and covariance matrix $t^2 I$ (here I is the identity matrix), then we use a local retraction β_x on \mathcal{M} in a neighbourhood of x to define the sample points $x_i = \beta_x(s_i)$.

Our method looks for a solution by parts, in which the singular points are the minimum points found until the last iteration. We update the size λ of the step in such way that after a certain number of iterations it decreases to a given proportion. We do this since the interval in which the curve is defined can be limited and by iterating with a fixed size we could get out. Therefore, if we take a smaller step size as the number of iterations increases, we obtain better estimates for the minimizer. Each time the number of iterations increases, we get closer to a local minimum. For this reason, our stopping criteria is determined when

$$|f(x_k) - f(x_{k+1})| \leq \epsilon,$$

for a certain accuracy ϵ . The latter will be called the *termination tolerance on the function value* and will be provided as an input parameter.

We summarize the above discussion in Algorithm 1.

Algorithm 1 Diffusion-map-based optimization

input Initial guess x_0 , gradient approximation parameter t , relaxation parameter λ , number of samples m , sub-iteration control number l , termination tolerance ϵ , and step-scale factor s_f .

initialization

$k \leftarrow 0$

$counter \leftarrow 0$

$x_{min} \leftarrow x_0$

$x_{-1} \leftarrow x_0$

while $|f(x_{k-1}) - f(x_k)| \geq \epsilon$ **or** $k = 0$

1. Generate multivariate random points $s_1, s_2 \cdots s_m$ with distribution $\mathcal{N}(x_k, t^2 I)$, where I is the n dimensional identity matrix
2. **for** $i = 1$ to m **do**
 - $s_i \leftarrow \beta_{x_k}(s_i)$
3. **end for**
4. $\bar{P}_t f(x_k) \leftarrow \frac{1}{m} \sum_{i=1}^m (s_i - x_k)(f(s_i) - f(x_k))$
5. $x_{k+1} \leftarrow \beta_{x_k}(x_k - \lambda \frac{\bar{P}_t f(x_k)}{t^2})$
6. **if** $f(x_{k+1}) < f(x_{min})$ **do**
 - $x_{min} \leftarrow x_{k+1}$
7. **end if**
8. $k \leftarrow k + 1$
9. **if** $l < counter$ **do**
 - $counter \leftarrow 0$
 - $x_k \leftarrow x_{min}$
 - $\lambda \leftarrow \lambda/s_f$
10. **end if**
11. $counter \leftarrow counter + 1$

end while

return x_{min}

5. Numerical Experiments and Applications

The following experiments were implemented in MATLAB software, using a desktop computer with the following configuration: Intel i5 9400 4.1 GHz processor, and 16 GB RAM.

As an elementary example, we use Algorithm 1 to find the smallest eigenvalue of a real symmetric $n \times n$ matrix A . We recall that the smallest eigenvalue is the minimum value of the function $f : S^{n-1} \rightarrow \mathbb{R}$ defined as

$$f(x) = \langle x, Ax \rangle.$$

In the following experiment we use as an example the matrix A defined by

$$\begin{bmatrix} 1 & 1 & 0 \\ 1 & -5 & 1 \\ 0 & 1 & 1 \end{bmatrix}.$$

We use Algorithm 1 with parameters $t = 10^{-5}$, $\lambda = 10$, $m = 100$, $l = 50$, $s_f = 1.1$, and discrepancy $Dis = 10^{-1}$. Here, we use the smooth retraction $\beta_{x_k}(z) = z/\|z\|$. In this experiment our initial point is

$$x_0 = \frac{1}{\sqrt{2}} \begin{bmatrix} -1 & -1 & 0 \end{bmatrix}.$$

In Figure 5.1, we plot the iterations given by our algorithm. The red point represents our initial point x_0 , and the blue point is our last iteration. In Figure 5.2, we plot the errors E and E_1 for three different executions. The error E is defined as

$$|f(x_k) - \gamma|,$$

where x_k is the k iteration, and γ is the smallest eigenvalue. This error measures how close the approximations are to the smallest eigenvalue. The error E_1 defined by

$$\|Ax_k - f(x_k)x_k\|,$$

measures how much the approximation x_k is an eigenvector of matrix A . Observe that when the number of iteration increases both errors converges to zero. This guarantees the convergence of this method. This example shows the effectiveness of our method

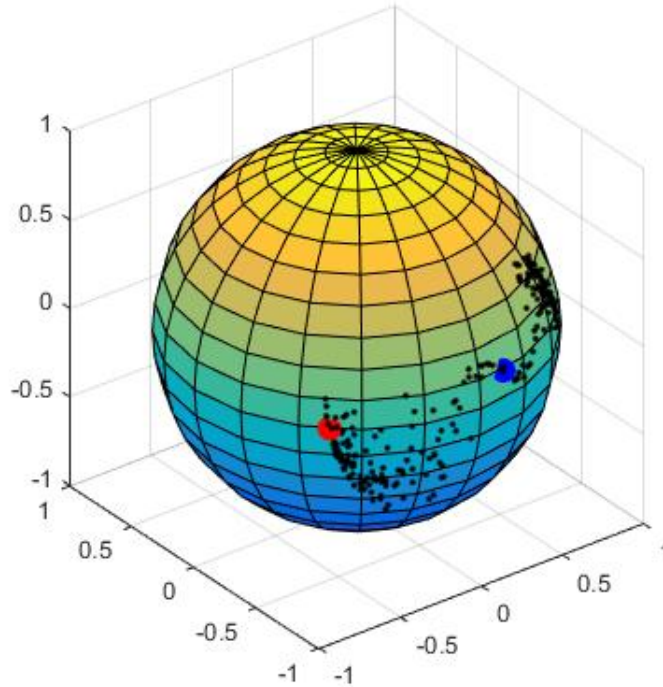
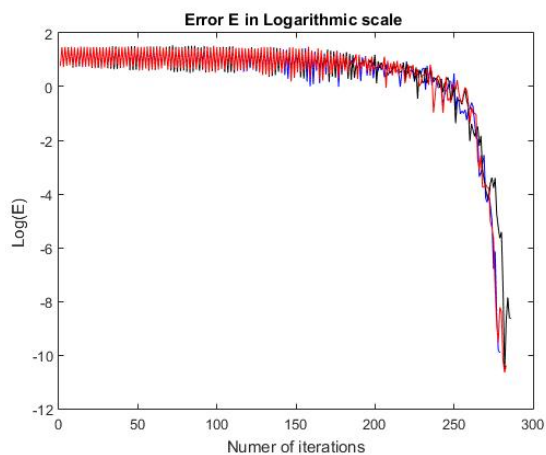


Figure 5.1: Execution of our method for the lowest eigenvalue of the matrix A . The red point represents our starting point, and the blue point the last iteration.

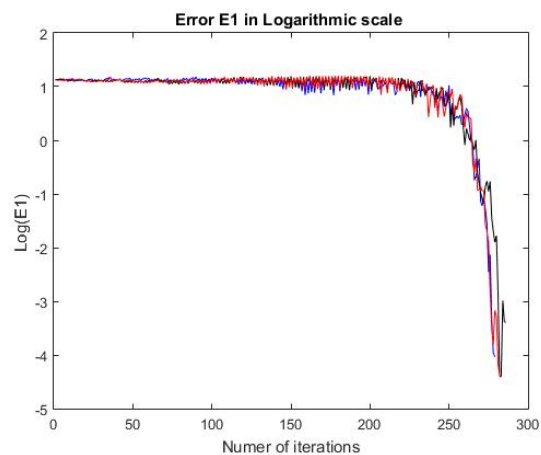
in optimizing functions over submanifolds. However, in numerical tests other classical methods to compute eigenvalues are carried out more quickly than the proposed here.

5.1. Sphere packing problem in dimensions 2 and 3

The sphere packing problem asks how to arrange congruent balls as densely as possible, such that at most touch each other on the boundary. This problem has exact solution in dimensions 1, 2, 3, 8, 24. The one dimensional sphere packing problem is the interval packing problem on the line, which is trivial. The two and three dimensional are far from trivial. The two dimensional case of packing circles in the plane was first solved in 1892 by the Norwegian mathematician Thue. He showed that the hexagonal packing gives the greatest density; see Figure 5.3. The three dimensional case of packing spheres in \mathbb{R}^3 was first posed by Johannes Kepler in 1611, so it is often referred to as the Kepler Conjecture. In 1831 Gauss proved that the pyramid arrangement of equally sized spheres filling space is optimal among lattice packings, but this still leaves out a lot of possible packings; see Figure 5.4. In 1900 Hilbert included this problem in his famous list of unsolved problems



(a) Eigenvector basis



(b) Real and imaginary part of the Fourier basis

Figure 5.2: Plot of the Errors E and E_1 , for three different executions. Note that errors are on logarithmic scale.

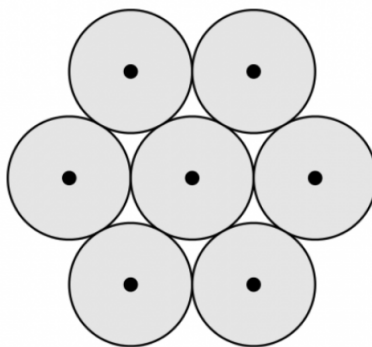


Figure 5.3: The hexagonal lattice and the corresponding sphere packing.

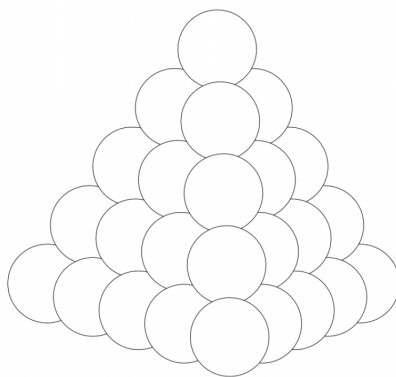


Figure 5.4: The pyramid sphere packing in \mathbb{R}^3 .

(as part of the 18th). The three dimensional problem was solved by Thomas Hales in 2005, he gave a complex proof, which makes intensive use of computers [14]. In 2017, Maryna Viazovska solved the problem in dimension eight and twenty four. See Refs. [15, 16].

A remarkable feature of this problem is that each dimension has its own peculiarities. It does not seem likely that a single and simple construction will give the best packing in every dimension.

We now discuss the problem with more details. We denote Vol the volume form associated with the Lebesgue measure, and for $x \in \mathbb{R}^n$ and r a positive real number, we denote by $B(x, r)$ the ball in \mathbb{R}^n with center x and radius r .

How do we define a sphere packing in the n dimensional space? To this end, we assume that $C \subset \mathbb{R}^n$ be a discrete set of points such that $2r \leq \|x - y\|$, for any two distinct $x, y \in C$, where r is a positive real number. Then, the union

$$S = \bigcup_{x \in C} B(x, r),$$

is a sphere packing, and its density Δ_S is define as

$$\Delta_S = \limsup_{r \rightarrow \infty} \frac{Vol(S \cap B(0, r))}{Vol(B(0, r))}.$$

Intuitively, the density of a sphere packing is the fraction of space covered by the spheres of the packing. The sphere packing problem consists in knowing what is the supremum Δ_n over all possible packing densities in \mathbb{R}^n . The number Δ_n is called the n dimensional sphere packing constant.

One important way to create a sphere packing is to start with a lattice $\Lambda \subset \mathbb{R}^n$, and center the spheres at the points of Λ , with radius half the length of the shortest non-zero vectors in Λ . Such a packing is called a lattice packing. A more general notion than a lattice packing is a periodic packing. In periodic packings, the spheres are centered on the points in the union of finitely many translates of a lattice Λ . Not every sphere packing is a lattice packing, and in fact in all sufficiently large dimensions, there are packings denser than every lattice packing. In contrast, it is proved in Ref. [17] that periodic packings get arbitrarily close to the greatest packing density. Moreover, in Ref. [17] it is shown that for every periodic packing P of the form

$$P = \bigcup_{i=1}^k \bigcup_{x \in \Lambda} (x_i + B(x, r)),$$

where Λ is a lattice, its density is given by

$$\Delta_P = k \frac{\text{Vol}(B(0, r))}{\text{Vol}(\Lambda)},$$

where $r = \min_{x, y \in P} \|x - y\|$. Our purpose in this experiment is to use our method to maximize the packing density over all lattice packings in dimensions 2 and 3. Observe that the density packing is invariant under scaling, that is, for a lattice Λ and a positive constant α we have $\Delta_{\alpha\Lambda} = \Delta_\Lambda$. Thus, without loss of generality and normalizing if necessary, we can assume that the volume of the lattice is $\text{Vol}(\Lambda) = 1$. If b_1, \dots, b_n is a basis for Λ , then our problem can be reformulated as

$$\begin{aligned} \max_{b_1, \dots, b_n} \quad & \text{Vol}(B(0, 1)) \left(\frac{g(b_1, \dots, b_n)}{2} \right)^n \\ \text{subject to} \quad & \det(b_1, \dots, b_n) = 1. \end{aligned} \tag{5.1}$$

where $\det(\cdot)$ is the determinant function, and the function $g(b_1, \dots, b_n)$ is defined as the minimum value of $\|z_1 b_1 + \dots + z_n b_n\|$ over all possible $(z_1, \dots, z_n) \in \mathbb{Z}^n \setminus 0$.

To apply our approach, we first prove that the function g is locally Lipschitz. To prove our claim we assume that a_1, \dots, a_n and b_1, \dots, b_n are vectors in \mathbb{R}^n such that $\det(a_1, \dots, a_n) = \det(b_1, \dots, b_n) = 1$. We write the matrices A and B as the column form $A = [a_1, \dots, a_n]$ and $B = [b_1, \dots, b_n]$. Observe that there exists an open set $U \ni A$ of the special linear group $SL(n)$, and a positive constant D such that for all $B \in U$

$$\|B^{-1}\| \leq D.$$

Assume that $g(a_1, \dots, a_n) = \|z_1 a_1 + \dots + z_n a_n\|$ for some $(z_1, \dots, z_n) \in \mathbb{Z}^n \setminus 0$. Then, we have that

$$g(b_1, \dots, b_n) - g(a_1, \dots, a_n) \leq \|A^{-1}\| \|A - B\| \|z_1 a_1 + \dots + z_n a_n\|.$$

Minkowski's theorem for convex bodies guarantees that for any matrix C with $\det(C) = 1$, the estimate $g(C) \leq \sqrt{n}$ is satisfied. Thus, we obtain that

$$g(b_1, \dots, b_n) - g(a_1, \dots, a_n) \leq \sqrt{n} D \|A - B\|.$$

By symmetry, the above inequality is still valid if we change the order of A and B . This

proves our claim.

In dimensions 2 and 3 the solutions of Problem 5.1 are $\Delta_2 = \frac{\pi}{2\sqrt{3}}$ and $\Delta_3 = \frac{\pi}{3\sqrt{2}}$, respectively. In these dimensions the maximizers are the hexagonal lattice, Figure 5.3, and the pyramid lattice packing, Figure 5.4.

Observe that Problem 5.1 can be considered as an optimization problem on the manifold $SL(n)$. We use our approach to find the maximizers in dimensions 2 and 3. Since maximizing the function g is equivalent to minimizing $-g$, then we apply our approach to the function $-g$. We use Algorithm 1 to the function $-g$. Since $\Delta_n \leq 1$, then, we take a small initial step size to get a better performance of our methodology. In these experiments our initial guess x_0 is the identity matrix and initial parameters $t = 10^{-5}$, $\lambda = 0.1$, $m = 50$, $l = 20$, $\epsilon = 10^{-10}$, $s_f = 1.1$. In this experiment, we use the local retraction

$$\beta_A(b_1, \dots, b_n) = \frac{(\text{sgn}(\det(B)) b_1, b_2, \dots, b_n)}{|\det(B)|^{\frac{1}{n}}}.$$

We emphasize that the parameters for which we obtain better results were those described above.

We use the Exhaustive Enumeration Algorithm proposed in Ref. [18] to compute the function g . The implementation of this algorithm is provided in the GitHub repository [19] using MATLAB.

We test our algorithm through five executions. In Figure 5.5, we plot the absolute error AE of approximating Δ_2 and Δ_3 for the iteration value x_n .

In Figures 5.6 and 5.7, we plot the final step of each execution of our algorithm in dimensions 2 and 3. Observe that in all executions, the final step approximates the optimal sphere packing in each dimension (to rotations). This fact was verified by calculating the error in the Figure 5.5.

5.2. Cryogenic electron microscopy

The Cryogenic electron microscopy (Cryo-EM) is a widely used technique in biology and medicine Refs. [20, 21, 22, 23, 24]. In recent years this technique has gained relevance in many scientific fields. In fact, in 2017 the Nobel Prize in Chemistry was awarded for developing Cryo-EM for the high-resolution structure determination of biomolecules in solution [25].

In Cryo-EM a particle is frozen and a series of tomographic projections are taken. The problem consists in the reconstruction of the three dimensional density of the particle using noise tomography projections. In contrast with classical tomography, in Cryo-EM

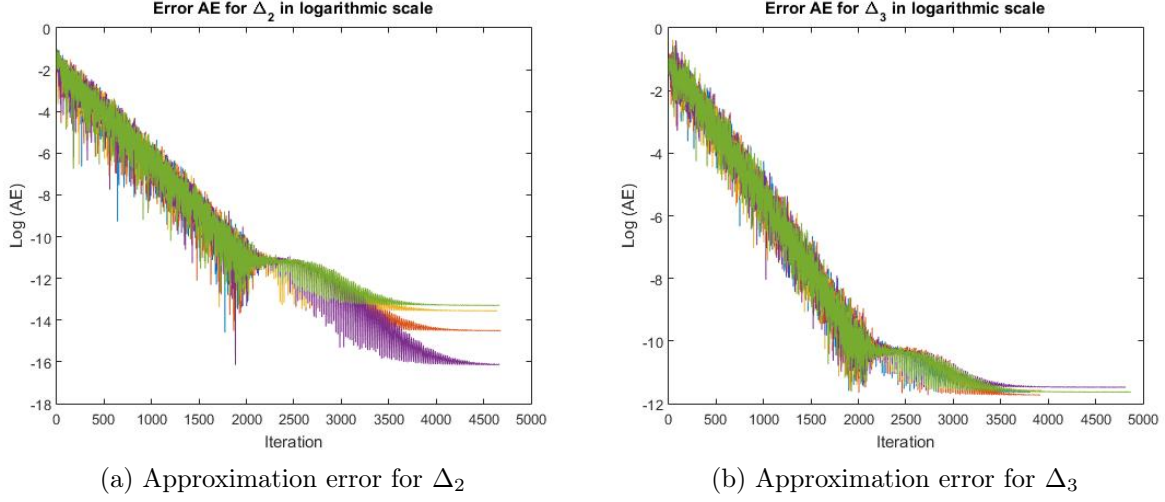


Figure 5.5: Plot of the absolute error (AE) generated by five approximations using Algorithm 1. Here we use the logarithmic scale.

the angular positions for which the projections are taken are unknown. Thus, Cryo-EM is a nonlinear inverse problem, which makes it more difficult compared to linear inverse problems.

Now, we explain the problem from a mathematical point of view. We refer the reader to Ref. [1] for more detailed information on the matter. Suppose that $f : \mathbb{R}^3 \rightarrow \mathbb{R}$ describes the density of a particle, and let R be a rotation in \mathbb{R}^3 . We define the two dimensional projection operator as

$$\mathbb{P}_R f(x, y) = \int f(R(x, y, z)) dz.$$

The Cryo-EM problem consists in reconstructing the density f with the knowledge of certain projections $\mathbb{P}_{R_1} f, \mathbb{P}_{R_2} f, \dots, \mathbb{P}_{R_k} f$. In this case, the rotations R_1, R_2, \dots, R_k are unknown. If through some method the rotations are known, then this inverse problem would be linear. In this case, we can obtain the density function f using classical reconstruction methods.

In Ref. [1] an approach is proposed to deal with this problem. This approach is based on using the common lines of the Fourier transform of the projections. To be more specific, the slice Fourier theorem states that

$$\mathcal{F}_2(\mathbb{P}_R)(x, y) = \mathcal{F}_3(f)(R(x, y)),$$

where \mathcal{F}_n is the n - dimensional Fourier transform. Since the intersection of two different

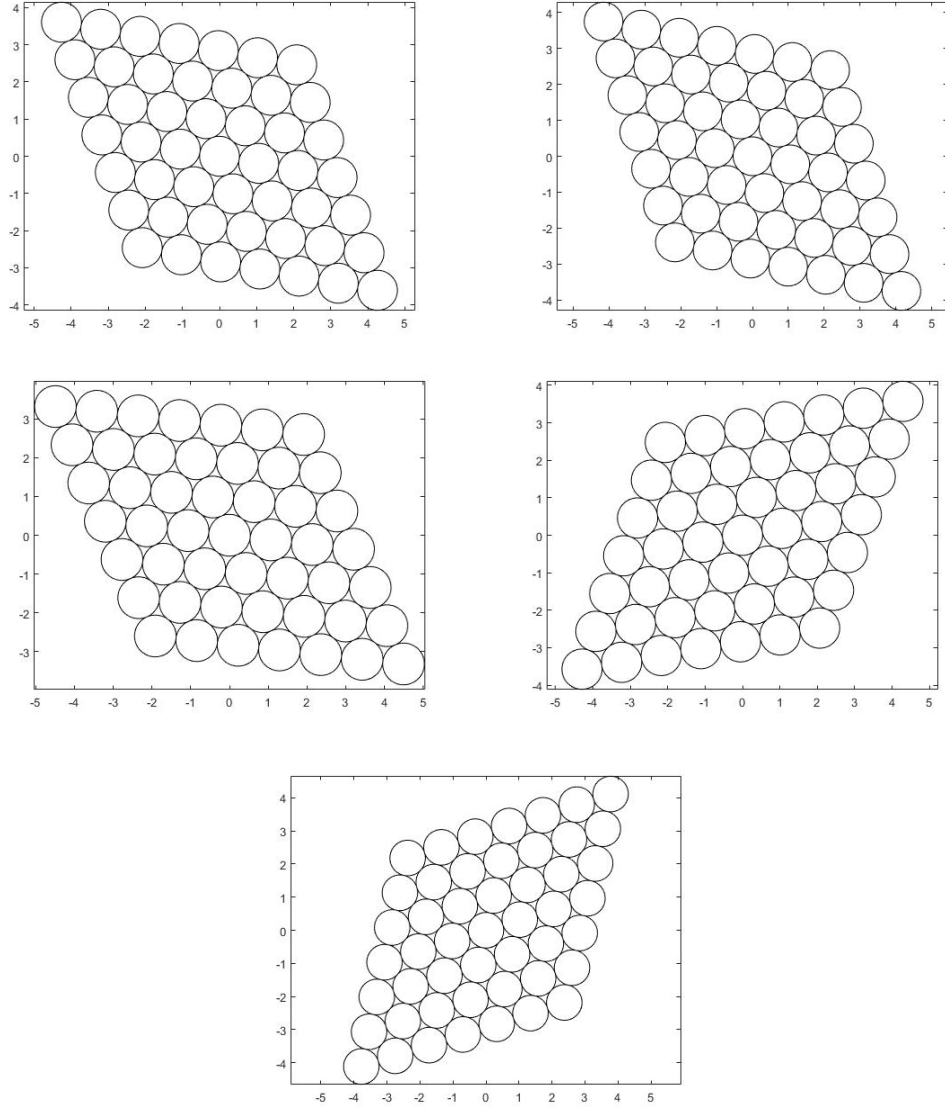


Figure 5.6: Plot of final lattice packing step of five executions to approximate the density Δ_2 .

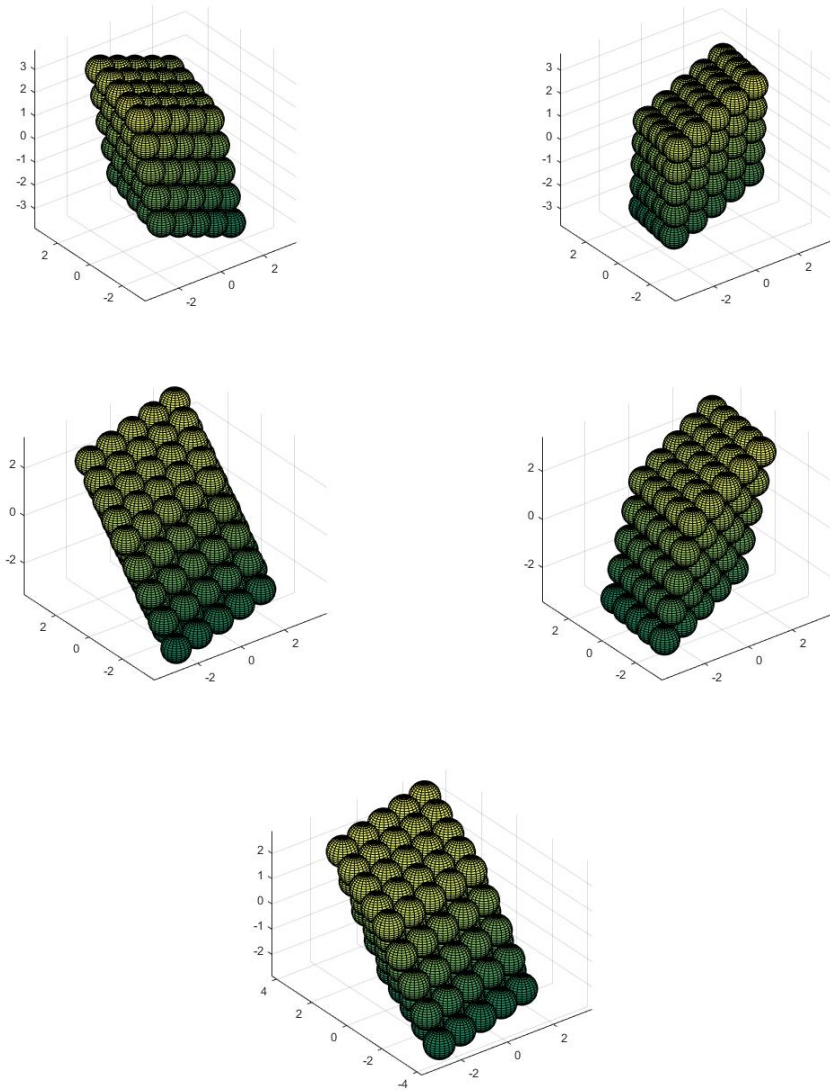


Figure 5.7: Plot of final lattice packing step of five executions to approximate the density Δ_3 .

planes is a common line, It is not difficult to verify that for $1 \leq i < j \leq k$ there exist unit vectors $v_{i,j}, v_{j,i} \in \mathbb{R}^2$ such that

$$R_i(v_{i,j}) = R_j(v_{j,i}).$$

In this case we have

$$\mathcal{F}_2(\mathbb{P}_{R_i})(v_{i,j}) = \mathcal{F}_2(\mathbb{P}_{R_j})(v_{j,i}),$$

the above equation allows to find the common lines between two projections. However, due to noisy measurements, the computation of common lines can be affected. In Ref. [26] a method to detect the common lines is proposed, this method is based on a voting system to eliminate false lines. Once the common lines are detected, it is possible to find the rotations R_1, R_2, \dots, R_k solving the optimization problem

$$\min_{R_1 R_2 \dots R_k \in SO(3)} \sum_{i < j} \|R_i(v_{i,j}) - R_j(v_{j,i})\|^2. \quad (5.2)$$

Problem 5.2 is not convex which makes it seriously difficult to solve. On the other hand, in Ref. [1] the authors do not focus on solving Problem 5.2, but instead solving another equivalent optimization problem. For that, the authors defined the matrix S as

$$\begin{bmatrix} S^{11} & S^{12} \\ S^{21} & S^{22} \end{bmatrix},$$

where S^{11}, S^{12}, S^{21} , and S^{22} are matrices with zero diagonal. These matrices are given by

$$S_{i,j}^{kl} = v_{i,j}(k)v_{j,i}(l),$$

for $1 \leq k, l \leq 2$ and $i \neq j$. Since S is a symmetric matrix, the authors used the first three eigenvectors to find an approximation $X_0 = (R_1^0, R_2^0, \dots, R_k^0)$ of the solution of Problem 5.2.

Now, we use our theory as post-processing tool. For that, we implement the Algorithm 1 to the function $h : SO(3) \times SO(3) \cdots \times SO(3) \rightarrow \mathbb{R}$ given by

$$h(R_1, R_2, \dots, R_k) = \sum_{i < j} \|R_i(v_{i,j}) - R_j(v_{j,i})\|^2. \quad (5.3)$$

The parameters we use are $t = 10^{-4}$, $\lambda = 1$, $m = 30$, $l = 20$, $\epsilon = 10^{-12}$, $s_f = 1.5$. In this case our retraction is given by the Gram-Schmidt orthogonalization process. Here, our initial point is the point X_0 . In this experiment, we use the density defined as the

characteristic function $f = \mathbb{1}_A$ of the set

$$A = B_2(0, 1) \cup B_1((1.4, 0, 0), 1/2) \cup B_1((0, 1, 1), 1) \cup B_1((0, -1, 1), 1),$$

where $B_p(x, r)$ is the ball in the norm L^p with center x , and radius r . The set A can be seen as the head of a mouse. We generate random rotations R_1, \dots, R_n to compute the two dimensional projections $\mathbb{P}_{R_1}f, \mathbb{P}_{R_2}f, \dots, \mathbb{P}_{R_k}f$. We add random noise to these projections, and we consider the data set of the form

$$\mathbb{P}_{R_i}^\varepsilon f = \mathbb{P}_{R_i}f + \varepsilon W,$$

where W is a white noise. Our purpose is to recover the density f , using the measurements $\mathbb{P}_{R_i}^\varepsilon f$. We do not focus on recover the common lines. Instead, we focus on the solution of Problem 5.2. For that, we add five percent of additive white noise, that is, we assume that $\varepsilon = 0.05$.

We compute the error generated when applying our post-processing tool. In Figure 5.8, we plot the error given by Function 5.3, when we implement our method for multiple random rotations. These rotations have a distribution that is approximately the normal distribution centered on the identity matrix, and variance parameter $\sigma^2 = 10$. In Figure 5.9, we plot the computation time in the execution of our algorithm. We remark that we obtained similar results to the previous ones using multiple executions of our method. Observing the computation time and the error, we conclude that using our post-processing tool we obtain a better result in the Cryo-EM problem reconstruction, with a relatively low computational cost.

Once the approximations for the rotations have been calculated, we proceed to reconstruct the density function f . We use the Landweber method to reconstruct the density. We implement this method with a total of ten numerical iterations. In Figure 5.10, we plot three different transverse sections of the reconstruction obtained. By transverse section, we refer to the intersection of the three dimensional particle with a plane. To measure the effectiveness of our method, we compare the L^2 error generated when reconstructing the particle in a certain transverse section. In Table 1 we compute this L^2 error. Note that for these transverse sections the implementation of our method improves image reconstruction.

As a final observation we say that in our experiments we used the Landweber method for reconstruction instead of the three-dimensional Fourier transform proposed in Ref. [1]. This

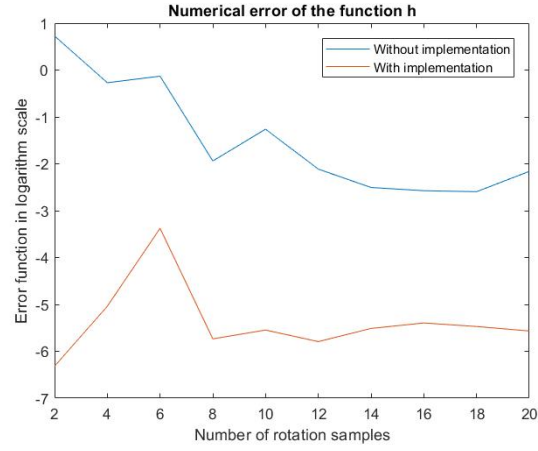


Figure 5.8: Plot of the error function h defined in Equation (5.3) using different number of samples. We use several values for the variance parameter $\sigma^2 = 10$.

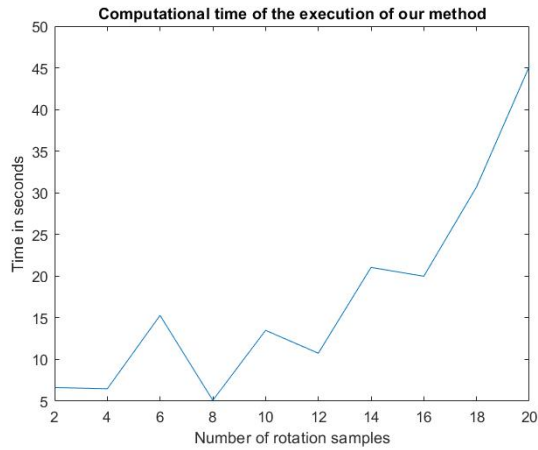


Figure 5.9: Plot of the computational time spent to run Algorithm 1 as a post-processing tool in Cryo-EM problem

| Transverse section | With implementation | Without implementation |
|--------------------|---------------------|------------------------|
| First | 3.5935 | 3.9711 |
| Second | 4.4517 | 4.9800 |
| Third | 4.0848 | 4.4644 |

Table 1: Error of three different sections. We use the L^2 norm to compute the errors. Here, the samples of random rotations are normally distributed with variance $\sigma^2 = 10$.

is because in this experiment the Landweber method provides better image reconstruction.

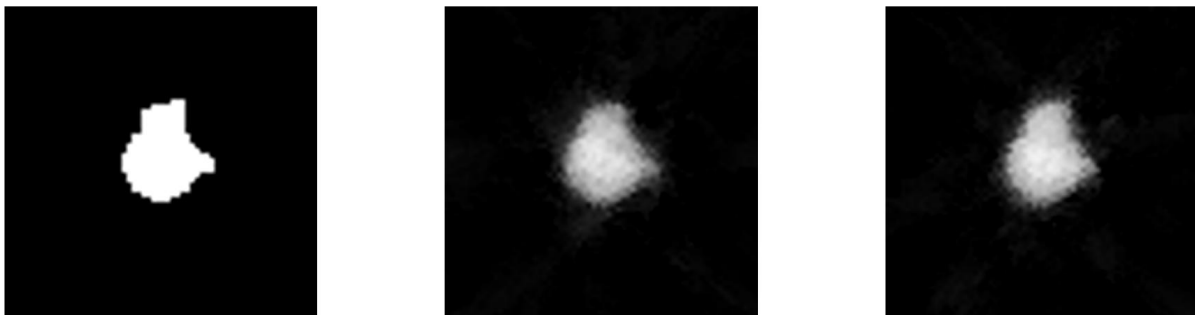
6. Conclusions

In this paper, we recover the gradient operator defined on Riemannian submanifolds of the Euclidean space from normally distributed random samples in a neighborhood of the point of interest. Our methodology is based on the estimates of the Laplace-Beltrami operator proposed in the diffusion maps approach. These estimates do not depend on the intrinsic dimension of the sub-manifold thus not suffering from the ‘‘curse of dimensionality.’’ This feature is useful in cases where it is not feasible to identify the dimension of the data set or in situations where we might want to scale up the dimension of the problem. Furthermore, a natural continuation of the present work would be to incorporate a non-linear dimensional reduction in the determination of the submanifold and in this case the aforementioned property would be very handy. Furthermore, this circle of ideas could be conjoined with the techniques proposed in [27].

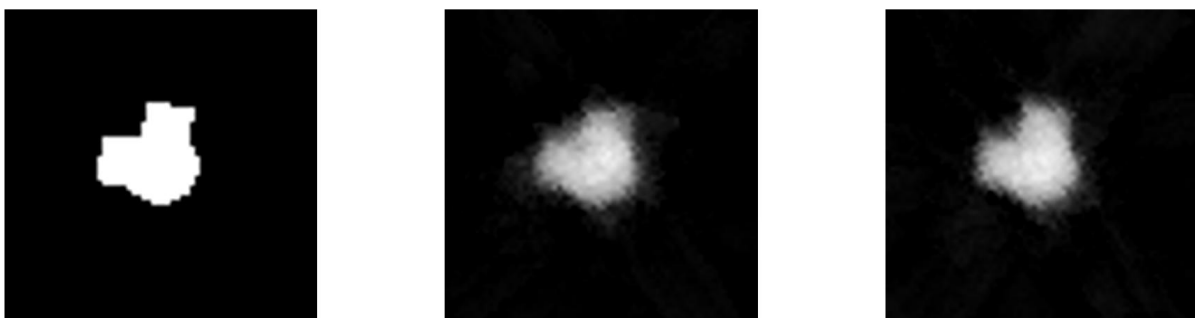
We apply our methodology in a step size algorithm as an optimization method on manifolds. This optimization method is effective in cases where it is difficult to compute the gradient of a function. As an application, we used our method to find an approximation to the sphere packing problem in dimension 2 and 3, for the lattice packing case. Moreover, we used our approach as a post-processing tool for the Cryo-EM problem. Our experiments indicate that this post-processing improves the reconstruction of the image.

A natural follow up is to apply this methodology to non-convex optimization problems in submanifolds, as well as high dimensional data sets. One consequence would be to use our approach as an iterative method to regularize nonlinear inverse problems in Euclidean submanifolds.

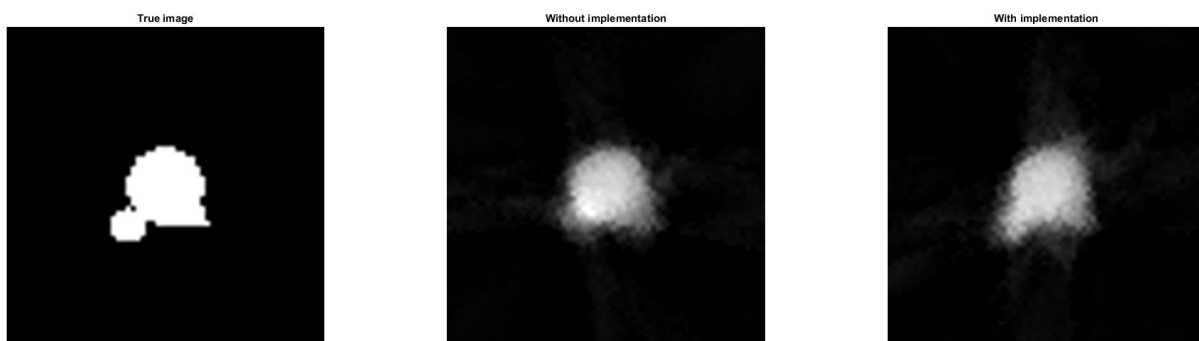
Due to the promising results obtained, a natural follow up would be to implement our algorithm in the case of periodic lattice packing to obtain computational estimates for the sphere packing constant in several dimensions.



(a) First transverse section



(b) Second transverse section



(c) Third transverse section

Figure 5.10: Plot of three different sections of the reconstructed images. The images on the left represent the true density function. The images on the center are obtained without the implementation of our algorithm, and the images on the right are obtained by implementing the algorithm. Here, the samples of random rotations are distributed according to the parameter $\sigma^2 = 10$.

We also plan to implement our method as a post-processing tool for other image reconstruction problems as well as integrating with other processing techniques such as for example the one described in [28].

Acknowledgements

The authors acknowledge the financial support provided by CAPES, Coordenação de Aperfeiçoamento de Pessoal de Nível Superior, grant number 88887.311757/2018-00, CNPq, Conselho Nacional de Desenvolvimento Científico e Tecnológico, grant numbers 308958/2019-5 and 307873/2013-7, and FAPERJ, Fundação Carlos Chagas Filho de Amparo à Pesquisa do Estado do Rio de Janeiro, grant numbers E-26/202.878/2017 and E-26/202.927/2017.

References

- [1] Amit Singer and Yoel Shkolnisky. Three-dimensional structure determination from common lines in cryo-em by eigenvectors and semidefinite programming. *SIAM journal on imaging sciences*, 4:543–572, 06 2011.
- [2] Joseph Frederic Bonnans, Jean Charles Gilbert, C Lemaréchal, and Claudia Sagastizabal. *Numerical Optimization – Theoretical and Practical Aspects*. Springer, 01 2006.
- [3] Silvére Bonnabel. Stochastic gradient descent on riemannian manifolds. *IEEE Transactions on Automatic Control*, 58, 11 2011.
- [4] Nilesh Tripuraneni, Nicolas Flammarion, Francis Bach, and Michael Jordan. Averaging stochastic gradient descent on riemannian manifolds. *Proceedings of the 31st Conference On Learning Theory*, 02 2018.
- [5] Sayan Mukherjee, Qiang Wu, and Ding-Xuan Zhou. Learning gradients on manifolds. *Bernoulli*, 16, 02 2010.
- [6] Ronald Coifman and Stéphane Lafon. Diffusion maps. *Applied and Computational Harmonic Analysis*, 21:5–30, 07 2006.
- [7] Ronald Coifman and Matthew Hirn. Diffusion maps for changing data. *Applied and Computational Harmonic Analysis*, 36:79–107, 01 2014.

- [8] Ronald Coifman, S. Lafon, Ann Lee, Mauro Maggioni, B. Nadler, F. Warner, and Steven Zucker. Geometric diffusions as a tool for harmonic analysis and structure definition of data. *Proceedings of The National Academy of Sciences - PNAS*, 102, 01 2005.
- [9] Alvaro Almeida Gomez, Antônio J. Silva Neto, and Jorge P. Zubelli. Diffusion representation for asymmetric kernels. *Applied Numerical Mathematics*, 166:208–226, 2021.
- [10] G. Malajovich and J. P. Zubelli. On the geometry of graeffe iteration. *Journal of Complexity*, 17(3):541–573, 2001.
- [11] G. Malajovich and J. P. Zubelli. Tangent graeffe iteration. *Numerische Mathematik*, 89(4):749–782, 2001.
- [12] Gerald Teschl. Ordinary differential equations and dynamical systems. *American Mathematical Society*, 01 2008.
- [13] Lawrence C. Evans. *Partial differential equations*. American Mathematical Society, Providence, R.I., 2010.
- [14] Thomas C. Hales. A proof of the kepler conjecture. *Annals of Mathematics*, 162(3):1065–1185, 2005.
- [15] Maryna Viazovska. The sphere packing problem in dimension 8. *Annals of Mathematics*, 185, 03 2016.
- [16] Henry Cohn, Abhinav Kumar, Stephen Miller, Danylo Radchenko, and Maryna Viazovska. The sphere packing problem in dimension 24. *Annals of Mathematics*, 185, 03 2016.
- [17] Helmut Groemer. Existenzsätze für lagerungen in metrischen räumen. *Monatshefte Fur Mathematik - MONATSH MATH*, 72:325–334, 08 1968.
- [18] Claus-Peter Schnorr and Martin Euchner. Lattice basis reduction: Improved practical algorithms and solving subset sum problems. *Mathematical programming*, 66(1-3):181–199, 1994.

- [19] Christian Chapman. *Implementation of shortest vector of a lattice using exhaustive enumeration*, 2018 (accessed December 20, 2018). <https://github.com/enthdegree/lenum.m>.
- [20] Richard Henderson. Model for the structure of bacteriorhodopsin based on high-resolution electron cryo-microscopy. *Ultramicroscopy*, 31:467–467, 12 1989.
- [21] Richard Henderson and P.N.T. Unwin. Henderson, r. unwin, p. n. t. three-dimensional model of purple membrane obtained by electron microscopy. *nature* 257, 28-32. *Nature*, 257:28–32, 10 1975.
- [22] Kazuyoshi Murata and Matthias Wolf. Cryo-electron microscopy for structural analysis of dynamic biological macromolecules. *Biochimica et Biophysica Acta (BBA) - General Subjects*, 1862, 07 2017.
- [23] Xiao-chen Bai, Greg McMullan, and Sjors Scheres. How cryo-em is revolutionizing structural biology. *trends biochem. Trends in Biochemical Sciences*, 40, 11 2014.
- [24] Tom Ceska, Chun-Wa Chung, Rob Cooke, Chris Phillips, and Pamela Williams. Cryo-em in drug discovery. *Biochemical Society Transactions*, 47:BST20180267, 01 2019.
- [25] Daniel Cressey and Ewen Callaway. Cryo-electron microscopy wins chemistry Nobel. *Nature*, 550(7675):167–167, October 2017.
- [26] Amit Singer, Ronald Coifman, Fred Sigworth, David Chester, and Yoel Shkolnisky. Detecting consistent common lines in cryo-em by voting. *Journal of structural biology*, 169:312–22, 11 2009.
- [27] Dmitry Pozharskiy, Noah J. Wichrowski, Andrew B. Duncan, Grigorios A. Pavliotis, and Ioannis G. Kevrekidis. Manifold learning for accelerating coarse-grained optimization. *Journal of Computational Dynamics*, 7(2):511–536, 2020.
- [28] J P Zubelli, R Marabini, C O S Sorzano, and G T Herman. Three-dimensional reconstruction by Chahine’s method from electron microscopic projections corrupted by instrumental aberrations. *Inverse Problems*, 19(4):933–949, jul 2003.
- [29] Manfredo P. do Carmo. *Riemannian Geometry*. Mathematics (Boston, Mass.). Birkhäuser, 1992.

Appendix A Review of differential geometry

We review some facts on differential geometry. We refer the reader to Ref. [29] for a more detailed description on the matter. Given an interior point $x \in \mathcal{M}$ there exists a positive real number ε such that the map $\psi = \exp_x \circ T : B(0, \varepsilon) \subset \mathbb{R}^d \rightarrow \mathcal{M}$ is a local chart. Where \exp_x is the exponential map at the point x , and $T : \mathbb{R}^d \rightarrow T_x\mathcal{M}$ is a rotation from \mathbb{R}^d onto $T_x\mathcal{M}$, both sets considered subsets of \mathbb{R}^n . The chart ψ defines the normal coordinates at point x .

Given a smooth function $f \in C^\infty(\mathcal{M})$, the gradient operator $\nabla f(x) \in T_x\mathcal{M}$ is given in normal coordinates by

$$\nabla f(x) = \sum_{i=1}^d \frac{\partial f}{\partial x_i} T(e_i).$$

Where e_i is the standard basis in \mathbb{R}^d . Now, we recall some estimates that use normal coordinates that are useful when estimating approximations for differential operators. The Taylor series of ψ around the point 0 is given by

$$\psi(v) = x + T(v) + \frac{1}{2} D^2 \psi_0(v, v) + O(\|v\|^3). \quad (\text{A.1})$$

Let $v \in B(0, \varepsilon) \subset \mathbb{R}^d$, and consider the geodesic $\gamma_{T(v)}$, with initial tangent vector $T(v) \in T_x\mathcal{M}$, then using Estimate A.1 we obtain

$$\gamma_{T(v)}(t) = x + T(v)t + \frac{1}{2} D^2 \psi_0(v, v)t^2 + O(\|v\|^3)t^3.$$

Since the covariant derivative of a geodesic vanishes, then $\gamma''_{T(v)}$ is orthogonal to $T_x\mathcal{M}$. Thus, we have the following estimates

$$\|\psi(v) - x\|^2 = \|T(v)\|^2 + O(\|v\|^4), \quad (\text{A.2})$$

and

$$\mathcal{P}_x(\psi(v) - x) = T(v) + O(\|v\|^3), \quad (\text{A.3})$$

where \mathcal{P}_x is the orthogonal projection on $T_x\mathcal{M}$. Using the Estimates A.2 and A.3, we obtain that there exist positive constants M_1 and M_2 such that for $\|v\|$ small

$$\|v\| - M_2\|v\|^3 \leq \|\psi(v) - x\| \leq M_1\|v\|.$$

Thus, if $\|v\|^2 \leq \frac{1}{2M^2}$ we have

$$\frac{1}{2}\|v\| \leq \|\psi(v) - x\| \leq M_1\|v\|.$$

This says that for t small

$$B(0, t/M_1) \subseteq \psi^{-1}(U(x, t^\delta)) \subseteq B(0, 2t). \quad (\text{A.4})$$

Appendix B Expansion of the Gradient operator

Here we show the technical details of the proof of Theorem 2.1, the main idea is to use the Taylor expansion of the function f around the point x .

Lemma B.1. *Assume that $\frac{1}{2} < \delta < 1$, and let $K : \mathcal{M} \times \mathcal{M} \rightarrow \mathbb{R}^m$ be a vector value kernel. Define*

$$P_t(x) = \int_{U(x, t^\delta)} K(x, y) e^{-\frac{\|y-x\|^2}{2t^2}} dy,$$

where $U(x, t^\delta)$ is defined as in Eq. (2.1). Assume that for t small, the function $\psi : B(0, 2t^\delta) \rightarrow \mathcal{M}$ defines normal coordinates in a neighbourhood of x , and let S be a vector value function defined in \mathbb{R}^d such that

$$K(x, \psi(v)) - S(v) = O(\|v\|^r),$$

and

$$K(x, y) = O(\|x - y\|^s).$$

Then, we have

$$P_t(x) = O((e^{C_2 t^{4\delta-2}} - 1)t^{s+d} + t^{r+d}) + \int_{\psi^{-1}(U(x, t^\delta))} S(v) e^{-\frac{\|T(v)\|^2}{2t^2}} dv.$$

Proof. Using (A.4), we assume that for t small, the set $U(x, t^\delta)$ lies in the image of a normal chart $\psi : B(0, 2t^\delta) \rightarrow \mathcal{M}$ centered in x . Thus

$$\begin{aligned} \int_{U(x, t^\delta)} K(x, y) e^{-\frac{\|y-x\|^2}{2t^2}} dy &= \int_{\psi^{-1}(U(x, t^\delta))} K(x, \psi(v)) e^{-\frac{\|\psi(v)-x\|^2}{2t^2}} dv \\ &= \int_{\psi^{-1}(U(x, t^\delta))} K(x, \psi(v)) (e^{-\frac{\|\psi(v)-x\|^2}{2t^2}} - e^{-\frac{\|T(v)\|^2}{2t^2}}) dv \\ &\quad + \int_{\psi^{-1}(U(x, t^\delta))} (K(x, \psi(v)) - S(v)) e^{-\frac{\|T(v)\|^2}{2t^2}} dv \\ &\quad + \int_{\psi^{-1}(U(x, t^\delta))} S(v) e^{-\frac{\|T(v)\|^2}{2t^2}} dv. \end{aligned}$$

We now estimate

$$A = \int_{\psi^{-1}(U(x, t^\delta))} K(x, \psi(v)) (e^{\frac{-\|\psi(v)-x\|^2}{2t^2}} - e^{\frac{-\|T(v)\|^2}{2t^2}}) dv.$$

Using Eq. (A.2), and the inequality $|e^x - 1| \leq e^{|x|} - 1$ we obtain

$$\begin{aligned} |e^{\frac{-\|\psi(v)-x\|^2}{2t^2}} - e^{\frac{-\|T(v)\|^2}{2t^2}}| &= e^{\frac{-\|T(v)\|^2}{2t^2}} |e^{\frac{O(\|v\|^4)}{2t^2}} - 1| \\ &\leq e^{\frac{-\|T(v)\|^2}{2t^2}} (e^{\frac{C_1\|v\|^4}{2t^2}} - 1). \end{aligned}$$

Therefore, by (A.4) we obtain

$$\begin{aligned} \|A\| &\leq C_3 t^s (e^{C_2 t^{4\delta-2}} - 1) t^d \int_{\mathbb{R}^d} \|v\|^s e^{-\|v\|^2/2} dv \\ &= O((e^{C_2 t^{4\delta-2}} - 1) t^{s+d}). \end{aligned}$$

On the other hand, by assumption we have

$$\int_{\psi^{-1}(U(x, t^\delta))} (K(x, \psi(v)) - S(v)) e^{\frac{-\|T(v)\|^2}{2t^2}} dv = O(t^{r+d}).$$

□

Lemma B.2. *Under the same assumptions of Lemma B.1, we define*

$$E = \int_{\psi^{-1}(U(x, t^\delta))} Q(v) e^{\frac{-\|T(v)\|^2}{2t^2}} g(v) dv,$$

where g is a smooth function and Q is a homogeneous polynomial of degree l . Then, we have

$$E = \int_{\mathbb{R}^d} Q(v) e^{\frac{-\|T(v)\|^2}{2t^2}} (g(0) + \sum \frac{\partial g}{\partial v_i}(0) v_i) dv + O(t^{d+l} e^{-M_2 t^{2(\delta-1)}} + t^{d+2+l}).$$

Proof. Using the Taylor expansion of g around 0 we have

$$E = \int_{\psi^{-1}(U(x, t^\delta))} Q(v) e^{\frac{-\|T(v)\|^2}{2t^2}} (g(0) + \sum \frac{\partial g}{\partial v_i}(0) v_i + O(\|v\|^2)) dv.$$

Let B be defined as

$$B = \left\| \int_{\mathbb{R}^d \setminus \psi^{-1}(U(x, t^\delta))} Q(v) e^{\frac{-\|T(v)\|^2}{2t^2}} (g(0) + \sum \frac{\partial g}{\partial v_i}(0) v_i) dv \right\|.$$

Using (A.4) and the fast decay of the exponential function, we obtain that

$$B \leq C_4 t^{d+l} e^{-M_2 t^{2(\delta-1)}} \int_{\mathbb{R}^d \setminus B(0, t^{\delta-1}/M_1)} P(\|v\|) e^{\frac{-\|T(v)\|^2}{4}} dv.$$

for a certain polynomial P . Therefore, we have

$$B = O(t^{d+l} e^{-M_2 t^{2(\delta-1)}}),$$

for a proper constant M_2 . Finally, we observe that

$$\int_{\psi^{-1}(U(x, t^\delta))} Q(v) e^{\frac{-\|T(v)\|^2}{2t^2}} O(\|v\|^2) dv = O(t^{d+2+l}).$$

□

We recall the following computations related to the moments of the normal distribution that are useful in proving Theorem 2.1. For all index i

$$\int_{\mathbb{R}^d} v_i e^{\frac{-\|T(v)\|^2}{2t^2}} dv = 0,$$

and

$$\int_{\mathbb{R}^d} v_i^2 e^{\frac{-\|T(v)\|^2}{2t^2}} dv = (2\pi)^{\frac{d}{2}} t^{d+2},$$

moreover, if $i \neq j$ then

$$\int_{\mathbb{R}^d} v_i v_j e^{\frac{-\|T(v)\|^2}{2t^2}} dv = 0.$$

Lemma B.3. *Under the same assumptions of Lemmas B.1 and B.2 we have*

$$d_t(x) = (2\pi)^{\frac{d}{2}} t^d + O(t^{d+F}),$$

for a positive constant F which only depends on δ .

Proof. We apply Lemmas B.1 and B.2 to the functions $K(x, y) = 1$, $S(v) = 1$, $Q(v) = 1$, and $g(x) = 1$. We use the parameters $r = 2$, $s = 0$ and $l = 0$. Using the exponential decay we obtain the following estimate

$$d_t(x) = (2\pi)^{\frac{d}{2}} t^d + O(t^{d+F}),$$

where F is the positive number defined as $F = \max(2 - 2\delta, 4\delta - 2)$.

□

Proof of Theorem 2.1. We apply Lemmas B.1 and B.2 to the functions $K(x, y) = (y - x)(f(y) - f(x))$, $S(v) = T(v)(f(\psi(v)) - f(x)) = \sum v_i(f(\psi(v)) - f(x))T(e_i)$, $Q(v) = v_i$ and $g(v) = (f(\psi(v)) - f(x))$. Since $\psi(v) - x - T(v) = O(\|v\|^2)$ and $f(\psi(v)) - f(x) = O(\|v\|^1)$, then the parameters that we use are $r = 3$, $s = 2$ and $l = 1$. Again, using the exponential decay we have that there exists a positive constant M such that

$$\int_{U(x, t^\delta)} \overline{K}(x, y) e^{\frac{-\|y-x\|^2}{2t^2}} dy = (2\pi)^{\frac{d}{2}} t^{d+2} \sum \frac{\partial f}{\partial v_i}(0) T(e_i) + O(t^{d+2+M}). \quad (\text{B.1})$$

Finally we use Lemma B.3 to conclude the result . □

E-mail address, Alvaro Almeida Gomez: `alvaro.gomez@ku.ac.ae`

E-mail address, Antônio J. Silva Neto: `ajsneto@iprj.uerj.br`

E-mail address, Jorge P. Zubelli: `zubelli@gmail.com`